KINETICS, CATALYSIS, AND REACTION ENGINEERING

Nonthermal Plasma Reactions of Dilute Nitrogen Oxide Mixtures: NO_x in Nitrogen

Gui-Bing Zhao,[†] Xudong Hu,[†] Man-Chung Yeung,[‡] Ovid A. Plumb,[§] and Maciej Radosz*,[†]

Department of Chemical & Petroleum Engineering, Department of Mathematics, and College of Engineering, University of Wyoming, Laramie, Wyoming 82071-3295

A lumped kinetic model of a pulsed corona discharge reactor, where the high-voltage discharge-induced electron density fluctuation and hence the electron collision rate fluctuation are approximated with a uniform electron distribution and a new Arrhenius-type rate model, is found to capture the effect of power input, NO_x composition, and residence time. An N atom and $N_2(A)$ are found to control the conversion of nitrogen oxides and the evolution of byproducts; the N atom controls the NO conversion, $N_2(A)$ controls the N_2O conversion, and the N atom and $N_2(A)$ control the NO_2 conversion.

Introduction

Flue gas streams contain ppm-level pollutants, such as NO_x and SO_x, which have to be removed or converted to benign species prior to discharge. One way to convert NO_x to nitrogen and oxygen is to expose the flue gas stream to an electric discharge, which generates radicals, ions, and excited molecules, which, in turn, activate the pollutants and convert them to benign stable species. Such a reactive mixture containing radicals, ions, and excited molecules in an otherwise neutral gas is referred to as plasma. If we apply a potential difference to plasma, the electric field will impart energy to the charged particles. The electrons, because of their small mass, will be immediately accelerated to a higher degree than the heavier ions between the collisions. If the pressure is low or the electric field is high or both, the electrons and ions will, on average, have a kinetic energy that is higher than the energy corresponding to the random motion of the molecules. Plasma in such a state is usually referred to as nonequilibrium plasma, where the highly energetic electrons are capable of ionizing and dissociating the neutral species at high rates even though the bulk gas temperature is quite low. Thus, it is said that such "cold nonequilibrium" discharges are capable of high-temperature chemistry at low temperatures. If, on the other hand, the pressure is so high that the charged particles do not move far between the collisions or the electric field is weak or both, the kinetic energy of the charged particles is not significantly different from the kinetic energy of the neutral species. We refer to such a plasma as equilibrium plasma.

In this work, we focus on a reactor in which nonthermal, nonequilibrium plasma is generated by high-voltage, short electric discharges. Such a reactor is commonly referred to as a pulsed corona discharge reactor (PCDR). The PCDR is characterized by a low gas temperature and a high electron energy, on the order of 5−10 eV.[1] Compared to other nonthermal plasma technologies using dc or ac corona discharge, PCDR was found to be energy efficient in a dry deNO_x/deSO_x process for utility thermal power plant boilers.[2] Corona discharge processes have been known for a long time[3] and studied for the conversion of nitrogen oxides,[1,2,4−10] sulfur dioxide,[11] and volatile organic carbons.[12]

Despite its technical potential, the nonthermal plasma reactions and their kinetics are poorly understood. This is because the parameter space of the design and operating variables is large.[13] Therefore, one needs a mathematical model that captures transport and reaction rates. Such a model is needed to develop new technologies and improve the existing plasma reactors. One of the major modeling challenges is to determine the rate of the electron collision reactions, which depends on the electron energy distribution.[4,5,13,14] The electron energy distribution can be estimated from the Boltzmann equation for a given electric field, which varies with time and gas composition. The previous modeling studies aimed at an approximate solution of the Boltzmann equation[13−15] suggest that this is a major challenge. As a result, the concentration of radicals, ions, and excited species and the rate constants of their reactions tend to be regressed from experimental data.[1,4]

A preliminary attempt at such a regression of the experimental data for nonthermal plasma reactions of NO_x in nitrogen was presented by Hu et al..[16] They used a time-averaged kinetic model, referred to as a lumped model, to fit experimentally determined product compositions by trial and error. They considered 10 reactions, including four electron collision reactions and six bulk reactions. A single set of rate parameters for those four electron collision reactions regressed for different reaction systems by Hu et al.,[16] however, cannot predict

* To whom correspondence should be addressed. Tel.: (307) 766-2500. Fax: (307) 766-6777. E-mail: radosz@uwyo.edu.
[†] Department of Chemical & Petroleum Engineering.
[‡] Department of Mathematics.
[§] College of Engineering.

10.1021/ie049934c CCC: $27.50
Published on Web 04/20/2004

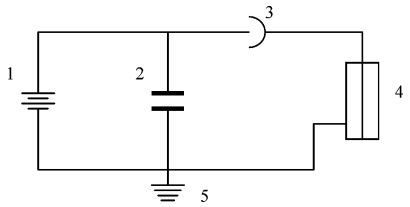

Figure 1. Schematic diagram of coaxial-type pulsed corona reactor: (1) power supply; (2) capacitor; (3) hydrogen switch; (4) positive PCDR; (5) grounding.

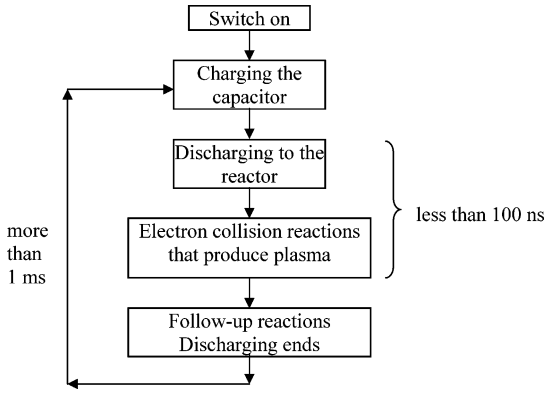

Figure 2. PCDR sequence.

byproduct N_2O concentration evolution in gas mixtures of NO + N_2 and byproduct NO concentration evolution in gas mixtures of NO_2 + N_2. The goal of this work, therefore, is to improve the model and to examine the chemical mechanism of nitrogen oxide conversion in the PCDR.

Experimental PCDR

An example of an experimental PCDR setup was presented by Hu et al.[17] A schematic diagram of the PCDR discharge process is shown in Figure 1, and that of the PCDR sequence is shown in Figure 2. After the reaction system is activated, the capacitor shown in Figure 1 is charged. Once the voltage on the capacitor is sufficiently high, a hydrogen spark gap switch connects the capacitor to the reactor anodes. The high voltage applied to the reactor anodes discharges energy to the gas flowing through the reactor, converting it to plasma. Once all of the capacitor energy is dissipated into the plasma, the discharge stops until a new pulse is initiated. The pulse repetition rate is controlled manually. The charge voltage is controlled with pressure in the hydrogen switch. The charge voltage of the capacitor, the discharge voltage, and the current to the reactor are measured with a digital oscilloscope (Tek Tronix TDS 784D). The average power delivered to the reactor gas is determined from the energy stored in the capacitor and the repetition rate. The PCDR effluent samples are collected in small stainless steel cylinders and analyzed for stable species by means of a Spectrum 2000 Perkin-Elmer Fourier transform infrared spectrometer with a narrow-band mercury−cadmium−telluride detector.

A fingerprint of the electron collision reactions in the PCDR is a plot of the discharge voltage and current versus time, for example, shown by Hu et al.[17] for pure nitrogen and argon. Such plots characterize the fluid ("streamer") properties around the point of discharge. As found by Creyghton et al.[18,19] and van Veldhuizen et al.,[20] the main properties of the streamer depend on

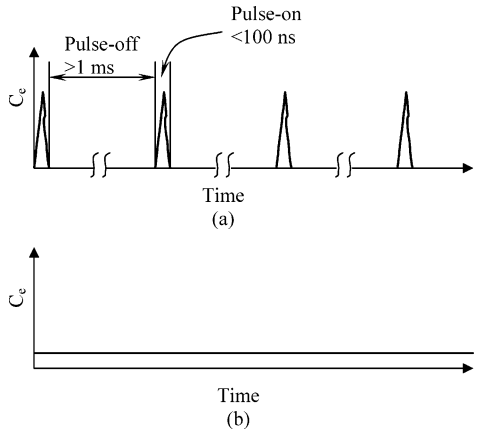

Figure 3. Distribution of the electron concentration: (a) real process; (b) lumped approximation.

the gas pressure and composition. These properties are reflected in the rise rate, the peak value of the applied voltage, and the pulse width (pulse duration).[21] In the example shown by Hu et al.,[17] the discharge is completed (discharge voltage or current reach zero) in less than 100 ns for the nitrogen system and in less than 30 ns for the argon system. However, the rise time for the discharge voltage and current is less than 15 ns in both cases. This implies that the electron collision reactions are completed in the initial 100 ns. Similar results were obtained by Tas et al..[22] Mok and Ham[7] found that the production of radicals by the electron collisions was completed in about 6 ns. However, the conventional pulse frequency in the PCDR is less than 1000 Hz. Therefore, the pulse-off time, defined as the time between the pulses and equal to the reciprocal of the pulse repetition rate, is on the order of 1 ms, which is much longer than the pulse-on time, as qualitatively shown in Figure 3a. This suggests that the electron collision reactions are likely to occur within the pulse-on period while the subsequent bulk reactions are likely to occur within the pulse-off period.

Two-Stage Model

On the basis of this hypothesis, most PCDR models are two-stage models: the electron collision reactions are the basis for calculating the concentration profile for the pulse-on stage, and the other reactions are the basis for calculating the concentration profile for the pulse-off stage. The total time for all two-stage events is made to match the reactor residence time.[1,4,7,9] For example, Penetrante et al.[9] applied the Boltzmann code called ELENDIF to obtain the ion and radical yields, which were used as input for describing the subsequent interaction of the ions and radicals with the exhaust gas. Mok et al.[1,7] adopted constant electron-induced dissociation constants, which were determined at a reduced electron field of 100 TD. The calculated concentrations of ions and radicals were used as input for the subsequent bulk reaction kinetics. Recently, Sathiamoorthy et al.[4] assumed that during the pulse-on period the electron concentration was fixed for the electron molecular collisions to calculate the concentration profile of different species. During the pulse-off period, the electron concentration was assumed to be zero. These two reaction sets, one with and one without the electrons present, were repeated to simulate the pulse-on and pulse-off periods and to match the residence time. However, because the discharge voltage and current

fluctuate, true temporal and spatial variations of the electron field and electron density are difficult to estimate realistically. Therefore, we prefer to build on a time-averaged model, referred to as the lumped model.

Lumped Model

The following seven assumptions are made in the lumped model used in this work:

(1) The electron density is evenly distributed in the reactor space and time. Figure 3b illustrates this approximation.

(2) All reactions occur throughout the reactor. Although evidence[23] suggests that free radicals may survive the plasma zone, the electron density approaches zero outside the plasma zone.

(3) The distribution of the electron velocity is Maxwellian. As a result, the rate constant for the electron collision reactions can be expressed as

$$k = \left(\frac{8k_B T_e}{\pi m_e}\right)^{1/2}\left(\frac{1}{k_B T_e}\right)^2 \int_0^\infty \left[E\sigma(E)\exp\left(\frac{-E}{k_B T_e}\right)\right] dE \quad (1)$$

(4) Following Huang and Suib,[23] we take the electron temperature to be proportional to the power input as follows:

$$k_B T_e = E^0 W/\alpha P \quad (2)$$

where E^0 is the threshold energy for an electron collision reaction to occur, P is the system pressure, W is the input power, and α is a constant of proportionality. The collision reaction cross section,[24] $\sigma(E)$ in eq 1, can be represented as

$$\sigma(E) = 0 \qquad \text{for } E \le E^0$$

$$\sigma(E) = b\left[1 - \frac{E^0}{E}\right] \qquad \text{for } E \ge E^0 \quad (3)$$

Combining eq 1 with eqs 2 and 3 yields

$$k = \beta_1\sqrt{\frac{W}{\alpha P}}\exp(-\alpha P/W) \quad (4)$$

where β_1 is a constant of proportionality. Thus, the rate constant for electron collision reactions is similar to the temperature dependence in the Arrhenius rate expression with power input in place of temperature. The parameter β_1 should capture the reactor and electrode geometry effects on the reaction rate, similar to that of the frequency factor in the Arrhenius rate expression. The effect of parameter α on the reaction rate is similar to that of the activation energy in the Arrhenius rate expression.

(5) The electron concentration is proportional to the power input raised to the uth power:

$$[e] = \beta_2 W^u \quad (5)$$

where u is derived from the experimental data and β_2 is a constant of proportionality. In our previous work,[17] on the basis of the experimental data on the conversion of N_2O, we found that $u = 0.25$. Thus, for electron collision reactions,

$$k[e] = \beta\sqrt{\frac{1}{\alpha P}}W^{0.75}\exp(-\alpha P/W) \quad (6)$$

where

$$\beta = \beta_1\beta_2 \quad (7)$$

(6) The reactor is isothermal, although in reality the corona discharge may slightly increase the reactor temperature.

(7) Axial dispersion is negligible, and hence the gas flow is plug flow.

On the basis of these approximations, we write a set of rate equations for all electron and bulk reactions

$$\begin{cases} \dfrac{dC_1}{dt} = \displaystyle\sum_{j=1}^{M}\phi_{1j}r_j = g_1(C_1,C_2,...,C_m;x_1,x_2,...,x_{2n};W_k) \\ \dfrac{dC_2}{dt} = \displaystyle\sum_{j=1}^{M}\phi_{2j}r_j = g_2(C_1,C_2,...,C_m;x_1,x_2,...,x_{2n};W_k) \qquad k = 1, 2, ..., L \\ \cdots\ \cdots\ \cdots\ \cdots\ \cdots \\ \dfrac{dC_m}{dt} = \displaystyle\sum_{j=1}^{M}\phi_{mj}r_j = g_m(C_1,C_2,...,C_m;x_1,x_2,...,x_{2n};W_k) \end{cases} \quad (8)$$

where C_i is the concentration of the species i ($i = 1, 2, ..., m$), t is the time, M is the total number of reactions, ϕ_{ij} is the stoichiometric coefficient of the ith species in the jth reaction, r_j is the reaction rate of the jth reaction ($j = 1, 2, ..., M$), n is the number of electron collision reactions, $x_1, x_2, ..., x_{2n}$ represent the $2n$ parameters α and β as shown in eq 6, and W_k ($k = 1, 2, ..., L$) is the power input for the kth experiment. Each experiment corresponds to a different concentration profile in the reactor because of a different power input.

The equation set (8) describes how the axial concentration profile for all species, including ions, radicals, molecules, and atoms, changes with the power input and residence time. The model parameters $x_1, x_2, ..., x_{2n}$ (i.e., α and β in our case) do not change with the pulse frequency and power input for a specific charge voltage and gas composition. These parameters are to be estimated using experimental data.

Objective Function

For a specific power input W_k, eq 8 can be integrated with respect to the residence time τ

$$\begin{cases} f_1^k(x_1,x_2,...,x_{2n}) = C_{1,\tau}^k - C_{1,0}^k - \displaystyle\int_0^\tau g_1^k(C_i^k,x_j,W_k)\,dt = 0 \\ f_2^k(x_1,x_2,...,x_{2n}) = C_{2,\tau}^k - C_{2,0}^k - \displaystyle\int_0^\tau g_2^k(C_i^k,x_j,W_k)\,dt = 0 \qquad i = 1, 2, ..., m \\ \cdots\ \cdots\ \cdots\ \cdots\ \cdots\ \cdots\ \cdots\ \cdots\ \cdots\ \cdots\ \cdots\ \cdots\ \cdots\ \cdots\ \cdots\ \cdots \qquad j = 1, 2, ..., 2n \\ f_m^k(x_1,x_2,...,x_{2n}) = C_{m,\tau}^k - C_{m,0}^k - \displaystyle\int_0^\tau g_m^k(C_i^k,x_j,W_k)\,dt = 0 \end{cases} \quad (9)$$

where $C_{i,\tau}^k$ and $C_{i,0}^k$ are the measured concentrations of the ith species at the outlet and inlet in the kth experiment, respectively; the integrals in eq 9 are for the concentration of all species C_i^k ($i = 1, 2, ..., m$). Equation 9 has n parameters α and n parameters β for n electron collision reactions. Because there are m equations for each power input, if we conduct L experiments at different power input levels, we end up with $L \times m$ equations.

Table 1. Experimental Matrix[a]

system	flow rate ($m^3 \cdot s^{-1}$)	reactor pressure (kPa)
NO conversion		
614 ppm of NO + N_2	4.18×10^{-4}	140.7*
600 ppm of NO + N_2	4.18×10^{-4}	140.7*
593 ppm of NO + N_2	2.15×10^{-4}	140.7
N_2O conversion		
275.6 ppm of N_2O + N_2	4.18×10^{-4}	140.7
275.6 ppm of N_2O + N_2	1.17×10^{-4}	140.7
96.6 ppm of N_2O + N_2	4.18×10^{-4}	140.7*
NO + N_2O mixture		
272 ppm of N_2O + 218 ppm of NO + N_2	4.18×10^{-4}	140.7
NO_2 conversion		
495 ppm of NO_2 + 800 ppm of O_2 + N_2	4.18×10^{-4}	140.7*

[a] New experimental data, except for those marked with asterisks, which were originally reported in ref 16 but have been corrected for this work.

The goal is to find a set of parameters x_j ($j = 1, 2, ..., 2n$) that minimize the objective function

$$G(x_1,x_2,...,x_{2n}) = \sum_{k=1}^{L} \sum_{i=1}^{m} |f_i^k(x_1,x_2,...,x_{2n})|^2 \qquad (10)$$

Finding its value at the point of minimum, min $[G(x_1,x_2,...,x_{2n})]$, is equivalent to a nonlinear optimization problem with $2n$ independent variables without constraints. A nonlinear numerical approach to solving this optimization problem to determine the model parameters α and β is described in the appendix. A Gear algorithm[7] is used for the integration of the system of stiff differential equations.

Results and Discussion

Reaction Analysis. Direct electron collision reactions with NO_x are deemed to be unimportant, and hence eliminated, primarily because of the very low concentration of NO_x. In real flue gas, as well as in our experimental gas mixtures, the concentration of NO_x is on the order of hundreds of ppm, which means a low probability of collision between electrons and NO_x. Therefore, we will only consider the electron collision reactions with nitrogen, which is the background gas.

On the basis of a preliminary analysis,[25] the N atom and the first excited state of nitrogen, $N_2(A)$, are found to be responsible for NO_x conversion in nonthermal nitrogen plasma. Therefore, two electron collision reactions

$$N_2 + e \rightarrow N + N + e \qquad (R1)$$

$$N_2 + e \rightarrow N_2(A) + e \qquad (R2)$$

are selected for further analysis.

To select other chemical reactions, we use experimental data shown in Table 1. All of these experiments were conducted in a four-tube reactor at a constant pressure of 140.7 kPa and a constant temperature of around 300 K. Among the main findings are the following: (1) ozone and oxides of nitrogen other than NO, NO_2, and N_2O were not detected; (2) for N_2O in N_2 experiments, only N_2O was detected; (3) for NO in N_2 and NO_2 in N_2 experiments, NO, NO_2, and N_2O were detected. Therefore, the reactions related to ozone and nitrogen oxides other than NO, NO_2, and N_2O are not considered in this study. On the basis of the prior work,[25] we select a total of 20 reactions that have large rate constants ($>10^{10}$ $cm^3 \cdot mol^{-1} \cdot s^{-1}$). These reactions are shown in Table 2. We analyze a total of 20 reactions for each NO_x in the N_2 system discussed below.

R4 is a three-body reaction whose pseudo-second-order rate constant depends on the temperature and pressure (concentration of the background gas),[26] as follows:

$$k = k_\infty \left(\frac{k_0/k_\infty}{1 + k_0/k_\infty} \right) \times 10^{(\log Fc)/\{1+[\log(k_0/k_\infty)/(0.75-1.27 \log Fc)]^2\}} \qquad (11)$$

Here, k_0 is the pseudo-second-order rate constant at a low-pressure limit, k_∞ is the second-order rate constant at a high-pressure limit, and log = $\log_{10}$. Fc is a function of temperature and is equal to 0.85 at 300 K.

NO in N_2 Reactions. There are four α and β parameters for the electron collision reactions R1 and R2. These parameters are determined from the NO-in-

Table 2. List of Possible Chemical Reactions for NO_x in N_2

chemical reaction	rate constant ($cm^3 \cdot mol^{-1} \cdot s^{-1}$)	source	no.
$N_2 + e \rightarrow N + N + e$	model parameters α_1 and β_1	this work	R1
$N_2 + e \rightarrow N_2(A) + e$	model parameters α_2 and β_2	this work	R2
$N + NO \rightarrow N_2 + O$	1.87×10^{13}	Atkinson et al.[34]	R3
$O + NO + N_2 \rightarrow NO_2 + N_2$	$k_0 = 3.62 \times 10^{16}$ [N_2] $k_\infty = 1.81 \times 10^{13}$ Fc = 0.85	Atkinson et al.[35]	R4
$NO_2 + N \rightarrow N_2O + O$	1.81×10^{12}	Atkinson et al.[34]	R5
$NO_2 + N \rightarrow N_2 + O_2$	4.21×10^{11}	Kossyi et al.[36]	R6
$NO_2 + N \rightarrow N_2 + 2O$	5.48×10^{11}	Kossyi et al.[36]	R7
$NO_2 + N \rightarrow 2NO$	1.38×10^{12}	Kossyi et al.[36]	R8
$NO_2 + O \rightarrow NO + O_2$	5.85×10^{12}	Atkinson et al.[35]	R9
$N_2(A) + NO \rightarrow N_2 + NO$	3.31×10^{13}	Herron and Green[37]	R10
$N_2(A) + N_2O \rightarrow 2N_2 + O$	3.73×10^{12}	Herron and Green[37]	R11
$N_2(A) + NO_2 \rightarrow N_2 + NO + O$	7.83×10^{12}	Herron and Green[37]	R12
$N_2(A) + O_2 \rightarrow N_2 + 2O$	1.51×10^{12}	Herron and Green[37]	R13
$N_2(A) + O_2 \rightarrow N_2O + O$	4.70×10^{10}	Kossyi et al.[36]	R14
$N_2(A) + O_2 \rightarrow N_2 + O_2$	7.77×10^{11}	Kossyi et al.[36]	R15
$N_2(A) + O \rightarrow N_2 + O$	1.81×10^{13}	Herron and Green[37]	R16
$N_2(A) + N \rightarrow N_2 + N$	2.71×10^{13}	Herron and Green[37]	R17
$N + N + N_2 \rightarrow N_2 + N_2$	1.59×10^{15} [N_2]	Kossyi et al.[36]	R18
$O + O + N_2 \rightarrow O_2 + N_2$	1.10×10^{15} [N_2]	Kossyi et al.[36]	R19
$N + O + N_2 \rightarrow NO + N_2$	3.68×10^{15} [N_2]	Kossyi et al.[36]	R20

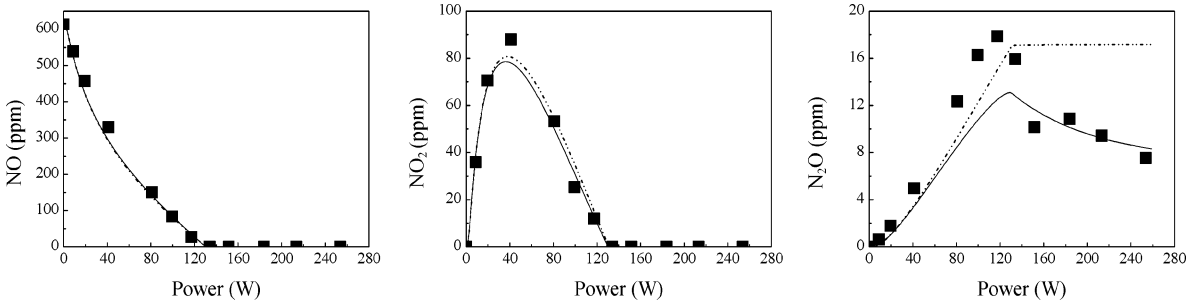

Figure 4. Experimental and correlated data for 614 ppm of NO in N_2 at 4.18×10^{-4} $m^3 \cdot s^{-1}$: (■) experimental data; (—) calculated data including two electron collision reactions R1 and R2; (-···-) calculated data including one electron collision reaction R1.

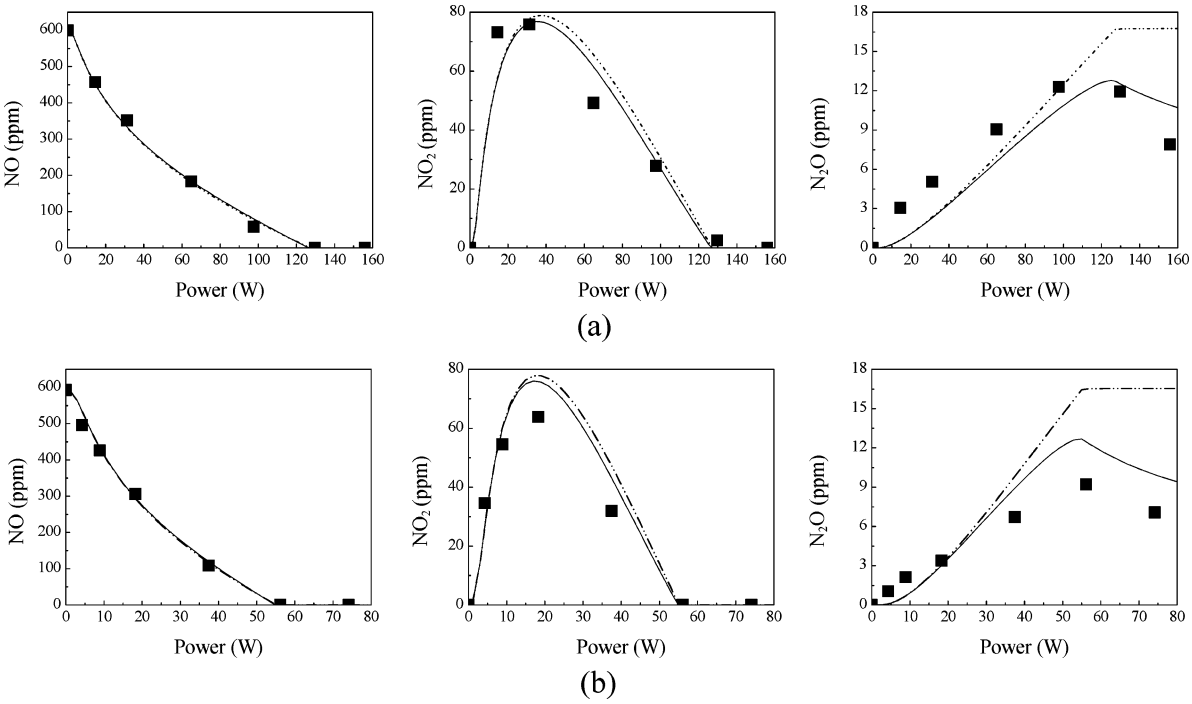

Figure 5. Experimental and predicted data for NO in N_2: (a) 600 ppm of NO in N_2, flow rate = 4.18×10^{-4} $m^3 \cdot s^{-1}$; (b) 593 ppm of NO in N_2, flow rate = 2.15×10^{-4} $m^3 \cdot s^{-1}$; (■) experimental data; (—) calculated data including two electron collision reactions R1 and R2; (-···-) calculated data including one electron collision reaction R1.

N_2 experimental data (11 power inputs) at 614 ppm of NO in N_2 and a flow rate of 4.18×10^{-4} $m^3 \cdot s^{-1}$. There are eight components (N_2, N, N_2(A), O, NO, NO_2, N_2O, and O_2) in this reaction system, as shown in Table 2. Therefore, there are eight equations for each power input, which leads to a total of 88 equations used to determine α and β. The concentration of N_2 and O_2 at the outlet of the reactor can be obtained using the nitrogen and oxygen material balance. Figure 4 shows NO, NO_2, and N_2O concentrations calculated for the experiment used in fitting α and β. It is not surprising that the calculated curves in Figure 4 reasonably represent the experimental data because these data have been used for fitting. The α and β values reported in Table 3 are used without further fitting for predicting the concentrations obtained in all of the other experiments at other power inputs, other initial NO concentrations, and other gas flow rates. The results are presented in Figure 5. These results suggest that a single set of α and β values derived from a single set of experimental data can predict the PCDR product compositions obtained at other conditions for the initial set of 20 reactions shown in Table 2. The residence time for the gas flow rate of 4.18×10^{-4} $m^3 \cdot s^{-1}$ and 600 ppm of NO in N_2 is almost half that for 2.15×10^{-4} $m^3 \cdot s^{-1}$ and 593 ppm of NO in N_2, but the predicted results shown in Figure 5 are still accurate. This suggests that the gas flow rate does not affect the gas discharge and plasma chemical reactions. The assumption of plug flow is therefore reasonable. In general, this model should be accurate up to a total of about 1000 ppm of NO and other nitrogen oxides. For a NO_x concentration higher than 1000 ppm, electron collisions with NO_x may become significant, and hence more electron collision reactions should be included. However, it is probably safe to extrapolate to higher power inputs, beyond the range used for fitting.

Table 3. Optimal Model Parameters

reaction system	model param	R1	R2	residual **G** (ppm)
$NO + N_2$	α	3.38	5.13	4.62
	β	5.12×10^{-6}	1.21×10^{-5}	
$NO_2 + O_2 + N_2$	α	3.79	5.86	11.9
	β	5.22×10^{-6}	9.92×10^{-6}	
$NO + N_2O + N_2$	α	3.46	5.23	8.22
	β	5.44×10^{-6}	1.24×10^{-5}	
$N_2O + N_2$	α	3.87	5.45	2.08
	β	1.64×10^{-5}	7.21×10^{-6}	

The previous investigators[1,4,6,7,9,16,22,27] concluded that the N atom is the only active species responsible for NO

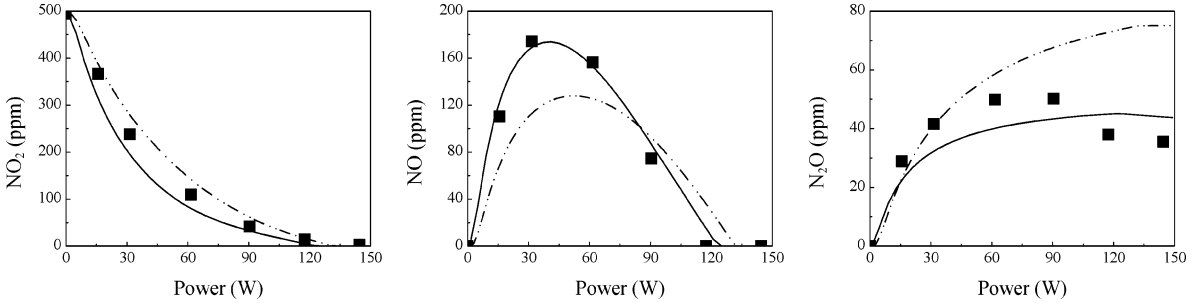

Figure 6. Experimental and predicted data for $NO_2 + O_2$ in N_2: (■) experimental data; (—) calculated data including two electron collision reactions R1 and R2; (-···-) calculated data including one electron collision reaction R1.

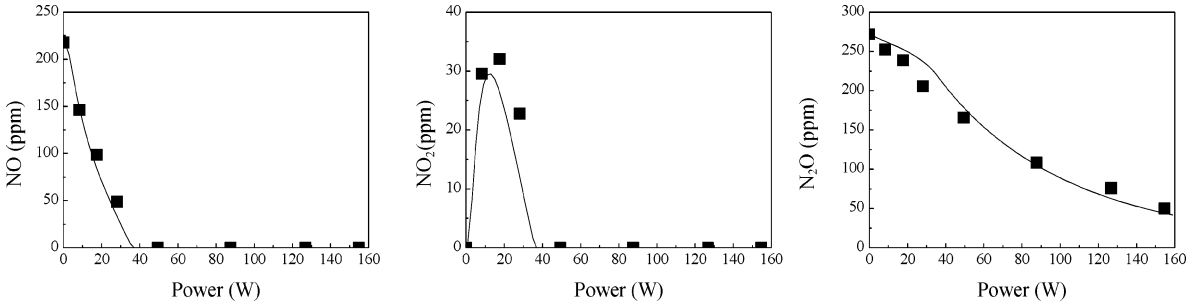

Figure 7. Experimental and predicted data for $NO + N_2O$ in N_2: (■) experimental data; (—) calculated data including two electron collision reactions R1 and R2.

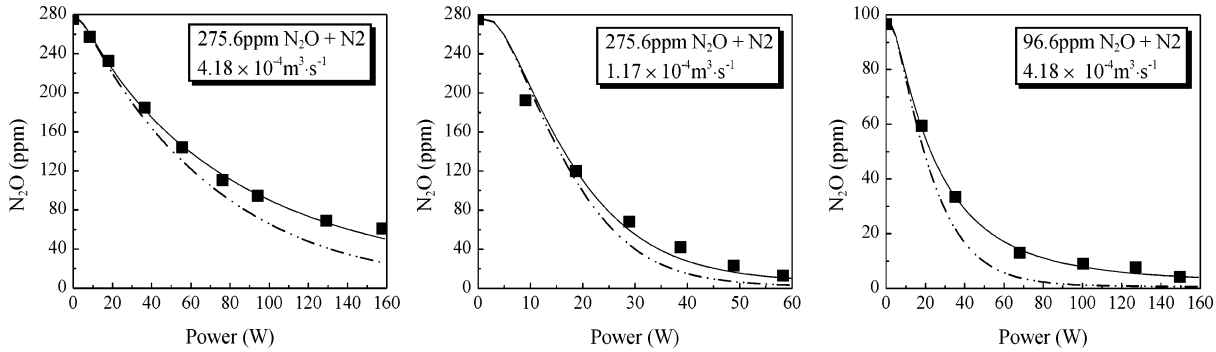

Figure 8. Experimental and predicted data for N_2O in N_2: (■) experimental data; (—) calculated data including two electron collision reactions R1 and R2; (-···-) calculated data including one electron collision reaction R2.

conversion and the formation of byproducts. This is represented by the dashed curve in Figures 4 and 5, where the electron collision reaction R2 is excluded. These results indicate that the exclusion of $N_2(A)$ does not affect the evolution of NO and NO_2 much, but it strongly affects the evolution of the byproduct N_2O. The experimental results shown in Figures 4 and 5 indicate that the byproduct N_2O initially increases with increasing power input, but then it decreases once NO is depleted. However, the calculated results without N_2-(A) indicate that N_2O remains constant once NO is depleted. This implies that both the N atom and $N_2(A)$ are important for NO conversion and for the formation and evolution of byproducts.

$NO_2 + O_2$ in N_2 Reactions. We determine the model parameters by solving 48 equations with four unknowns for eight species (N_2, N, $N_2(A)$, O, NO, NO_2, N_2O, and O_2) and six power inputs. The optimal model parameters are shown in Table 3. The results shown in Figure 6 suggest a good agreement with the experimental data.

If we only consider the electron collision reaction R1, as was done by Hu et al.,[16] the NO and N_2O concentration profiles cannot be predicted, as illustrated in Figure 6 (dashed curve). This indicates that both the N atom (R5−R8) and $N_2(A)$ (R12) are important for NO_2 conversion and for the formation and evolution of byproducts.

NO and N_2O in N_2 Reactions. We determine the model parameters by solving 56 equations with four unknowns for eight species (N_2, N, $N_2(A)$, O, NO, NO_2, N_2O, and O_2) and seven power inputs. The optimal model parameters are shown in Table 3, and the results are shown in Figure 7. Once again, we obtain a good agreement with the experimental data.

N_2O in N_2 Reactions. If we consider all 20 reactions presented in Table 2, we end up with eight equations with four parameters describing the evolution of eight species (N_2, N, $N_2(A)$, O, NO, NO_2, N_2O, and O_2) for any specific power input. We use the experimental results for 275.6 ppm of N_2O in N_2 at 4.18×10^{-4} $m^3 \cdot s^{-1}$ to fit the model parameters. This means that we have 64 equations with four unknown parameters to be determined. The optimal α and β parameters are shown in Table 3. These parameters are used to predict the experimental concentrations of all species at other operating conditions, including variation of the gas velocities, initial reactant concentrations, and power inputs. Figure 8 suggests a good agreement between the predicted and experimental data. As found earlier for

NO conversion, the gas flow rate does not affect the gas discharge and plasma chemical reactions. For example, the gas residence time at 4.18×10^{-4} $m^3 \cdot s^{-1}$ is almost 4 times lower than that at 1.17×10^{-4} $m^3 \cdot s^{-1}$ for 275.6 ppm of N_2O in N_2, but the predicted results shown in Figure 8 are still in good agreement with the experimental data, which further justifies the plug-flow assumption.

We do not detect NO and NO_2 in the N_2O conversion experiments. The calculated concentrations of NO and NO_2 at all conditions shown in Figure 8 are lower than 0.04 ppm, which explains our experimental observation. Similar results were reported by Futamura et al.[6]

Figure 8 also shows calculated results excluding the electron collision reaction R1 (dashed curve). The corresponding conversion rate of N_2O is higher than that observed experimentally, especially at high power input, because the N atom accumulates and quenches $N_2(A)$ (R17), which suppresses N_2O conversion. These results suggest that the contribution of the N atom is important in N_2O conversion.

As shown in Table 3, the model parameters α and β for R1 and R2 obtained for the three reaction systems, $NO + N_2$, $NO_2 + O_2 + N_2$, and $NO + N_2O + N_2$, are found to be nearly the same. This suggests that the electron collision reaction rates for these systems are nearly the same. However, this is not the case for $N_2O + N_2$, where β for R1 is higher than that for the other systems and β for R2 is lower than that for the other systems. This is because, in the reaction system of $N_2O + N_2$, there is no strong quencher, such as NO. $N_2(A)$, therefore, is likely to accumulate in the reactor and be converted to the N atom, which can be explained with two possible mechanisms. One is a stepwise dissociation of nitrogen:

$$N_2 + e \rightarrow N_2(A) + e \qquad \text{(R2)}$$

$$N_2(A) + e \rightarrow N + N + e \qquad \text{(R21)}$$

The other, as suggested by Gordiets et al.,[28] Brovikova and Galiaskarov,[29] and Guerra et al.,[30] is as follows:

$$N_2(A) + N_2(A) \rightarrow N_2 + 2N \qquad \text{(R22)}$$

$$N_2(A) + N_2(\mathbf{X}, 14 \le v \le 19) \rightarrow N_2 + 2N \qquad \text{(R23)}$$

Here, $N_2(\mathbf{X}, 14 \le v \le 19)$ is the vibrational state of N_2.

Conclusions

A lumped kinetic model is found to accurately represent experimentally determined compositions of dilute nitrogen oxide mixtures flowing through a pulsed corona reactor. Two rate parameters for each electron collision reaction, fitted to one set of experimental data, are found to predict the experimental data at other process conditions, including variations in the power input, NO_x composition (say, up to 1000 ppm), and residence time for each NO_x system.

The N atom and $N_2(A)$ are found to control the conversion of nitrogen oxides and the evolution of byproducts: the N atom controls the NO conversion, $N_2(A)$ controls the N_2O conversion, and both the N atom and $N_2(A)$ control the NO_2 conversion.

Acknowledgment

Dr. Pradeep K. Agarwal, who initiated this work, passed away in 2002. His influence and contributions are recognized and remembered. Drs. M. J. Biggs, T. M. Linjewile, J. Hamann, S. Mukhnahallipatna, and J. J. Zhang contributed to the earlier stages of this program.[16,17] Dr. S. Legowski and R. Borgialli provided experimental assistance. The authors also gratefully acknowledge the comments by Drs. H. Adidharma and M. Argyle that enhanced this manuscript. This work was funded by the National Science Foundation (Grants CTS 9810040 and CTS 0078700) and the Department of Defense (ARO-DAAD19-01-1-0488). Matching support was provided by the Research Office, University of Wyoming.

Appendix: Optimization Method

For convenience, we define a vector $\mathbf{X}$

$$\mathbf{X} = (x_1, x_2, ..., x_{2n})^T$$

where superscript T implies the transpose, and a new function $F(X)$

$$\mathbf{F}(X) = \{ f_1^1(X), f_2^1(X), ..., f_m^L(X)\}^T$$

Equation 10 can be rewritten as follows:

$$\mathbf{G}(X) = \mathbf{F}^T(X) \cdot \mathbf{F}(X) \qquad \text{(A1)}$$

According to the extreme value theorem, a differentiable single-variable function can have a relative minimum only when its derivative is zero. The gradient for a multivariable function is analogous to the derivative of a single-variable function. Therefore, a differentiable multivariable function can have a relative minimum at $\mathbf{X}$ only when its gradient is zero.[31] If we define the Jacobian matrix $\mathbf{A}$

$$\mathbf{A} = \begin{bmatrix} \frac{\partial f_1^1}{\partial x_1} & \frac{\partial f_1^1}{\partial x_2} & \cdots & \frac{\partial f_1^1}{\partial x_{2n}} \\ \frac{\partial f_2^1}{\partial x_1} & \frac{\partial f_2^1}{\partial x_2} & \cdots & \frac{\partial f_2^1}{\partial x_{2n}} \\ \cdots & \cdots & \cdots & \cdots \\ \frac{\partial f_m^L}{\partial x_1} & \frac{\partial f_m^L}{\partial x_2} & \cdots & \frac{\partial f_m^L}{\partial x_{2n}} \end{bmatrix} \qquad \text{(A2)}$$

then the gradient vector of $\mathbf{G}(X)$ is

$$\mathbf{\Gamma}(X) = \nabla \mathbf{G}(X) = \frac{\partial \mathbf{G}(X)}{\partial X} = 2\mathbf{A}^T(X) \cdot \mathbf{F}(X) \qquad \text{(A3)}$$

where

$$\frac{\partial \mathbf{G}(X)}{\partial X} = \left\{ \frac{\partial \mathbf{G}(X)}{\partial x_1}, \frac{\partial \mathbf{G}(X)}{\partial x_2}, ..., \frac{\partial \mathbf{G}(X)}{\partial x_{2n}} \right\}^T$$

The partial derivatives in eq A2 can be derived from eq 9

$$\frac{\partial f_i^k}{\partial x_j} = -\int_0^\tau \frac{\partial g_i^k(C_i^k; x_1, x_2, ..., x_j, ..., x_{2n}; W_k)}{\partial x_j} \, dt$$

$$\approx -[\int_0^\tau g_i^k(C_i^k; x_1, x_2, ..., x_j + \Delta x_j, ..., x_{2n}; W_k) \, dt - \int_0^\tau g_i^k(C_i^k; x_1, x_2, ..., x_j, ..., x_{2n}; W_k) \, dt]/\Delta x_j \qquad \text{(A4)}$$

and calculated using a finite-difference technique.

To implement these ideas numerically, we consider an arbitrary point $\mathbf{X}_l$ and a vector $\mathbf{P}_l$. The Taylor series gives the expansion of the gradient function (eq A3) at $\mathbf{X}_{l+1} = \mathbf{X}_l + \mathbf{P}_l$ as

$$\mathbf{\Gamma}_{l+1} = \mathbf{\Gamma}(\mathbf{X}_l+\mathbf{P}_l) = \mathbf{\Gamma}_l + \nabla^2\mathbf{G}\cdot\mathbf{P}_l \tag{A5}$$

because higher-order derivative terms are zero. If $\mathbf{X}_{l+1}$ is to be the minimum of the function $\mathbf{G}(X)$, then $\mathbf{\Gamma}_{l+1}$ must be zero and $\mathbf{P}_l$ is then given by

$$\mathbf{P}_l = -(\nabla^2\mathbf{G})^{-1}\cdot\mathbf{\Gamma}_l \tag{A6}$$

where $\mathbf{\Gamma}_l$ means $\mathbf{\Gamma}(\mathbf{X}_l)$ and $\nabla^2\mathbf{G}$, the second derivative of $\mathbf{G}(X)$, is the $2n \times 2n$ symmetric Hessian matrix of $\mathbf{G}(X)$. The element of $\nabla^2\mathbf{G}(X)$ is

$$\frac{\partial^2 G}{\partial x_i \partial x_j} = 2\sum_{s=1}^{L}\sum_{v=1}^{m}\left[\frac{\partial f_v^s}{\partial x_i}\frac{\partial f_v^s}{\partial x_j} + f_v^s\frac{\partial^2 f_v^s}{\partial x_i\,\partial x_j}\right] \tag{A7}$$

If we define a $2n \times 2n$ matrix $\mathbf{B}$ as

$$\mathbf{B} = \sum_{s=1}^{L}\sum_{v=1}^{m}[f_v^s\cdot\nabla^2 f_v^s] \tag{A8}$$

where $\mathbf{B}$ is the sum of the Hessian matrices of the individual subfunctions, each weighted by the value of its subfunction, then from eq A7, we have

$$\nabla^2\mathbf{G} = 2(\mathbf{A}^{\mathrm{T}}\cdot\mathbf{A} + \mathbf{B}) \tag{A9}$$

Substituting eqs A3 and A9 into eq A6, we have

$$\mathbf{P}_l = -[2(\mathbf{A}_l{}^{\mathrm{T}}\cdot\mathbf{A}_l + \mathbf{B}_l)]^{-1}\cdot 2\mathbf{A}_l{}^{\mathrm{T}}\cdot\mathbf{F}_l \tag{A10}$$

As proposed by Scales,[32] the $\boldsymbol{B}$ matrix is assumed to be negligible. Equation A10 leads to a small residual algorithm in Newton's method. Thus, we get

$$\mathbf{P}_l = -[\mathbf{A}_l{}^{\mathrm{T}}\cdot\mathbf{A}_l]^{-1}\cdot\mathbf{A}_l{}^{\mathrm{T}}\cdot\mathbf{F}_l \tag{A11}$$

Recognizing that the Jacobian matrix $\mathbf{A}$ is the $(m \times L) \times 2n$ unsymmetric matrix (in most cases, $m \times L \neq 2n$), we introduce a generalized inverse matrix of A

$$[\mathbf{A}_l{}^{\mathrm{T}}\cdot\mathbf{A}_l]^{-1} = \mathbf{A}_l{}^{+}\cdot(\mathbf{A}_l{}^{\mathrm{T}})^{+} \tag{A12}$$

and

$$(\mathbf{A}_l{}^{+})^{+} = \mathbf{A}_l \tag{A13}$$

where the superscript $+$ indicates the generalized inverse matrix of $\mathbf{A}$, which has properties similar to those of the inverse of a symmetric matrix. Thus, eq A11 becomes

$$\mathbf{A}_l\cdot\mathbf{P}_l = -\mathbf{F}_l \tag{A14}$$

In general, this is an overdetermined system of equations, which has a least-squares solution,[33] where one minimizes the sum of squares of residual errors between the right- and left-hand sides of eq A14.

Because the correction vector $\mathbf{P}_l$ is based on local information, the new approximation may have undesirable properties. For example, even though $\mathbf{P}_l$ is not uphill at $\mathbf{X}_l$, we may still find that $\mathbf{G}_{l+1} > \mathbf{G}_l$. It is necessary, therefore, to introduce a factor, $\boldsymbol{\lambda}_l$, that modifies the norm of the correction vector; we refer to the latter as a "search direction". $\boldsymbol{\lambda}_l$ is usually called a step length, or a "damping factor". Therefore, the iteration formula is

$$\mathbf{X}_{l+1} = \mathbf{X}_l + \boldsymbol{\lambda}_l\cdot\mathbf{P}_l \tag{A15}$$

If the gradient $\nabla\mathbf{G}(X)$ approaches zero, $|\Delta\mathbf{G}_l/\mathbf{G}_l|$ will be near zero, which is a convergence criterion for the iteration.

Specific numerical steps are as follows:

(1) Input the initial values X_0 of the $2n$ variables. Set $l = 0$, tolerance E for iteration convergence, and the maximum number of iterations N.

(2) If $l \leq N$, do steps 3−7.

(3) Calculate $\mathbf{A}_l$, $\mathbf{F}_l$, and $\mathbf{G}_l$.

(4) Calculate $\mathbf{P}_l$ using a least-squares method from eq A14.

(5) Find a damping factor $\boldsymbol{\lambda}_l$ using the method of a rational extreme value until the function of one-variable $\mathbf{G}_{l+1}$ arrives at a minimal value.

(6) If $|(\mathbf{G}_{l+1} - \mathbf{G}_l)/\mathbf{G}_l| < \mathbf{E}$, output $\mathbf{X}_l$ and $\mathbf{G}_l$. Stop.

(7) Set $l = l + 1$ and $\mathbf{X}_{l+1} = \mathbf{X}_l + \boldsymbol{\lambda}_l\cdot\mathbf{P}_l$.

(8) Output "maximum iterations exceeded" (procedure completed unsuccessfully). Stop.

Step 8 is rare. This method is found to exhibit rapid convergence. A Fortran code has been developed in this work for the algorithm described above.

Notation

$\mathbf{A}$ = Jacobian matrix
b = constant of proportionality in eq 3
$\mathbf{B}$ = sum of the Hessian matrices
C_e = concentration of the electron, mol·cm^{-3}
C_i = concentration of species i, mol·cm^{-3}
E^0 = threshold energy of the electron collision reaction, J
E = kinetic energy of electrons, J
k = rate constant, cm^3·mol^{-1}·s^{-1}
k_B = Boltzmann constant, 1.381×10^{-23} J·K^{-1}
l = number of iteration
m_e = electron mass, kg
P = system pressure, Pa
$\mathbf{P}_l$ = iteration vector of the lth step
r_j = reaction rate of the jth reaction, mol·cm^{-3}·s^{-1}
t = time, s
T_e = electron temperature, K
W = power input, J·s^{-1}
$\mathbf{X}$ = vector space of model parameters
x_i = model parameters, the same as α and β of the ith electron collision reaction

Greek Letters

α = constant of proportionality, model parameters
β_1 = constant of proportionality
β_2 = constant of proportionality
β = constant of proportionality ($\beta_1\beta_2$), model parameters
ϕ_{ij} = stoichiometric coefficient of the ith species in the jth reaction
τ = residence time, s
$\boldsymbol{\lambda}$ = damping factor
σ = collision cross section of the reaction, m^2

Literature Cited

(1) Mok, Y. S.; Ham, S. W.; Nam, I. S. Mathematical Analysis of Positive Pulsed Corona Discharge Process Employed for Removal of Nitrogen Oxides. *IEEE Trans. Plasma Sci.* **1998**, *26*, 1566−1574.

(2) Masuda, S. Report on novel dry DeNOx/DeSOx technology for cleaning combustion gases from utility thermal power plant boilers. In *Nonthermal Plasma Techniques for Pollutuion Control: Part B*; Penetrante, B. M., Schultheis, S. E., Eds.; Springer-Verlag: Berlin, 1993.

(3) Chang, J. S.; Lawless, P. A.; Yamamoto, T. Corona Discharge Processes. *IEEE Trans. Plasma Sci.* **1991**, *19*, 1152−1166.

(4) Sathiamoorthy, G.; Kalyana, S.; Finney, W. C.; Clark, R. J.; Locke, B. R. Chemical Reaction Kinetics and Reactor Modeling of NOx Removal in a Pulsed Streamer Corona Discharge Reactor. *Ind. Eng. Chem. Res.* **1999**, *38*, 1844−1855.

(5) Lowke, J. J.; Morrow, R. Theoretical Analysis of Removal of Oxides of Sulphur and Nitrogen in Pulsed Operation of Electrostatic Precipitators. *IEEE Trans. Plasma Sci.* **1995**, *23*, 661−671.

(6) Futamura, S.; Zhang, A.; Yamamoto, T. Behavior of N_2 and Nitrogen Oxides in Nonthermal Plasma Chemical Processing of Hazardous Air Pollutant. *IEEE Trans. Ind. Appl.* **2000**, *36*, 1507−1514.

(7) Mok, Y. S.; Ham, S. W. Conversion of NO to NO_2 in Air by a Pulsed Corona Discharge Process. *Chem. Eng. Sci.* **1998**, *53*, 1667−1678.

(8) Mok, Y. S.; Kim, J. H.; Nam, I. S.; Ham, S. W. Removal of NO and Formation of Byproducts in a Positive-Pulsed Corona Discharge Reactor. *Ind. Eng. Chem. Res.* **2000**, *39*, 3938−3944.

(9) Penetrante, B. M.; Hsiao, M. C.; Merritt, B. T.; Vogtlin, G. E.; Wallman, P. H. Comparison of Electrical Discharge Techniques for Nonthermal Plasma Processing of NO in N_2. *IEEE Trans. Plasma Sci.* **1995**, *23*, 679−687.

(10) Luo, J.; Suib, S. L.; Marquez, M.; Hayashi, Y.; Matsumoto, H. Decomposition of NOx with Low-Temperature Plasmas at Atmospheric Pressure: Neat and in the Presence of Oxidants, Reductants, Water, and Carbon Dioxide. *J. Phys. Chem. A* **1998**, *102*, 7954−7963.

(11) Clements, J. S.; Mizuno, A.; Finney, W. C.; Davis, R. H. Combined removal of sulfur dioxide, nitrogen oxides (NOx), and fly ash from simulated flue gas using pulsed streamer corona. *IEEE Trans. Ind. Appl.* **1989**, *25*, 62−69.

(12) Yamamoto, T.; Ramanathan, K.; Lawless, P. A.; Ensor, D. S.; Newsome, J. R.; Plaks, N.; Ramsey, G. H. Control of volatile organic compounds by an a.c. energized ferroelectric pellet reactor and a pulsed corona reactor. *IEEE Trans. Ind. Appl.* **1992**, *28*, 528−534.

(13) Graves, D. B.; Jensen, K. F. A Continuum Model of DC and RF Discharges. *IEEE Trans. Plasma Sci.* **1986**, *PS-14*, 78−91.

(14) Mukkavilli, S.; Lee, C. K.; Varghese, K.; Tavlarides, L. L. Modeling of the Electrostatic Corona Discharge Reactor. *IEEE Trans. Plasma Sci.* **1988**, *16*, 652−660.

(15) Naidis, G. V. On Streamer Interaction in a Pulsed Positive Corona Discharge. *J. Phys. D: Appl. Phys.* **1996**, *29*, 779−783.

(16) Hu, X.; Zhang, J.-J.; Mukhnahallipatna, S.; Hamann, J.; Biggs, M. J.; Agarwal, P. Transformations and destruction of nitrogen oxides—NO, NO_2 and N_2O—in a pulsed corona discharge reactor. *Fuel* **2003**, *82*, 1675−1684.

(17) Hu, X.; Nicholas, J.; Zhang, J. J.; Linjewile, T. M.; de Filippis, P.; Agarwal, P. K. The Destruction of N_2O in a Pulsed Corona Discharge Reactor. *Fuel* **2002**, *81*, 1259−1268.

(18) Creyghton, Y. M.; van Veldhuizen, E. M.; Rutgers, W. R. Streamer characteristics of Positive Pulsed Corona. 10th International Symposium on Plasma Chemistry, Bochum, Germany, 1991.

(19) Creyghton, Y. L. M.; van Bladel, F. M. A. M.; van Veldhuizen, E. M. Electrical and Spectroscopic Investigation of Pulsed Positive Streamer Corona in O_2-N_2 and CO_2-O_2 Mixtures. 3rd International Symposium on High Pressure, Low-Temperature Plasma Chemistry, Strasbourg, France, 1991.

(20) van Veldhuizen, E. M.; Creyghton, Y. L. M.; Rutgers, W. R. High-Resolution Schlieren Study of Pulsed Corona. Proceedings of the 4th International Conference on ESP, Beijing, China, 1990.

(21) Hackam, R.; Akiyama, H. Air Pollution Control by Electrical Discharges. *IEEE Trans. Dielectr. Electr. Insul.* **2000**, *7*, 654−683.

(22) Tas, M. A.; van Hardeveld, R.; van Veldhuizen, E. M. Reactions of NO in a Positive Streamer Corona Plasma. *Plasma Chem. Plasma Process.* **1997**, *17*, 371−391.

(23) Huang, J.; Suib, S. L. Dimerization of Methane through Microwave Plasmas. *J. Phys. Chem.* **1993**, *97*, 9403−9407.

(24) Butt, J. B. *Reaction Kinetics and Reactor Design*, 2nd ed.; Marcel Dekker: New York, 2000.

(25) Zhao, G. B.; Hu, X.; Argyle, M. D.; Radosz, M. N Atom and $N_2(A^3\Sigma_u^+)$ Found to be Responsible for Nitrogen Oxides Conversion in Nonthermal Nitrogen Plasma. *Ind. Eng. Chem. Res.* **2004**, submitted for publication.

(26) Troe, J. Analysis of the Temperature and Pressure Dependence of the Reaction $HO + NO_2 + M \leftrightarrow HONO_2 + M$. *Int. J. Chem. Kinet.* **2001**, *33*, 878−889.

(27) Hazama, H. F. M.; Tanimoto, M. Removal processes of nitric oxide along positive streamers observed by laser-induced fluorescence imaging spectroscopy. *Chem. Phys. Lett.* **2000**, *323*, 542−548.

(28) Gordiets, B.; Ferreira, C. M.; Pinheiro, M. J.; Ricard, A. Self-consistent kinetic model of low-pressure N_2-H_2 flowing discharges: I. Volume processes. *Plasma Sources Sci. Technol.* **1998**, *7*, 363−378.

(29) Brovikova, I. N.; Galiaskarov, E. G. Kinetic characteristics of production and loss of nitrogen atoms in N_2 plasma. *High Temp.* **2001**, *39*, 809−814.

(30) Guerra, V.; Galiaskarov, E.; Loureiro, J. Dissociation mechanisms in nitrogen discharges. *Chem. Phys. Lett.* **2003**, *371*, 576−581.

(31) Burden, R. L.; Faires, J. D. *Numerical Analysis*, 4th ed.; PWS−Kent Publishing Co.: Boston, 1989.

(32) Scales, L. E. *Introduction to Non-Linear Optimization*; Springer-Verlag: New York, 1985.

(33) Zhao, G. B.; Chen, J. Z.; Yang, Y. R. Predictive Model and Deterministic Mechanism in a Bubbling Fluidized Bed. *AIChE J.* **2001**, *47*, 1524−1532.

(34) Atkinson, R.; Baulch, D. L.; Cox, R. A.; Hampson, J. R. F.; Kerr, J. A.; Troe, J. Evaluated Kinetic and Photochemical Data for Atmospheric Chemistry: Supplement III. *J. Phys. Chem. Ref. Data* **1989**, *18*, 881−1097.

(35) Atkinson, R.; Baulch, D. L.; Cox, R. A.; Hampson, J. R. F.; Kerr, J. A.; Rossi, M. J.; Troe, J. Evaluated Kinetic and Photochemical Data for Atmospheric Chemistry: Supplement VI. *J. Phys. Chem. Ref. Data* **1997**, *26*, 1329−1499.

(36) Kossyi, I. A.; Kostinsky, A. Y.; Matveyev, A. A.; Silakov, V. P. Kinetic Scheme of the Non-equilibrium Discharge in Nitrogen−Oxygen Mixtures. *Plasma Sources Sci. Technol.* **1992**, *1*, 207−220.

(37) Herron, J. T.; Green, D. S. Chemical Kinetics Database and Predictive Schemes for Nonthermal Humid Air Plasma Chemistry. Part II. Neutral Species Reactions. *Plasma Chem. Plasma Process.* **2001**, *21*, 459−481.

Received for review January 20, 2004
Revised manuscript received March 2, 2004
Accepted March 10, 2004

IE049934C